# We are IntechOpen, the world's leading publisher of Open Access books Built by scientists, for scientists

**4,800**
Open access books available

**122,000**
International authors and editors

**135M**
Downloads

Our authors are among the

**154**
Countries delivered to

**TOP 1%**
most cited scientists

**12.2%**
Contributors from top 500 universities

CLARIVATE ANALYTICS BOOK CITATION INDEX INDEXED

WEB OF SCIENCE™

Selection of our books indexed in the Book Citation Index in Web of Science™ Core Collection (BKCI)

## Interested in publishing with us?
## Contact book.department@intechopen.com

Numbers displayed above are based on latest data collected.
For more information visit www.intechopen.com

# 12

# Artificial Neural Networks and Retinal Ganglion Cell Responses

María P. Bonomini[3], José M. Ferrández[1,2] and Eduardo Fernández[1]
[1]*Instituto de Bioingeniería, Universidad Miguel Hernández, Elche,*
[2]*Dept. Electrónica y Tecnología de Computadores, Univ. Politécnica de Cartagena,*
[3]*CEBBAD, Universidad Maimónides,*
[1,2]*Spain*
[3]*Argentina*

## 1. Introduction

Our continuous perception of the world, our sensations about light, colour, music, speech, taste, smell is turned into and coded as binary data by the peripheral sensory systems, and sent by the corresponding nerves to the brain where this code is interpreted and coloured with emotions. The binary sensory data consists in sequences of identical voltage peaks, called action potentials or spikes. Seeing consists in decoding the patterns of these spike trains which are sent to the brain, via the optic nerve, by the visual transduction element: the retina. The external world object features, such as size, colour, intensity, are transformed by the retina in a myriad of parallel spikes sequences, which must describe with precision and robustness all the characteristics perceived. Getting insight into this population code is, nowadays, a basic question for visual science.

A considerable number of coding studies have focused on single ganglion cell responses. Traditionally, the spiking rate of aisle cells has been used as an information carrier due to the close correlation with the stimulus intensity in all sensory systems. There are, however some drawbacks when analysing single cell firings. Firstly, the response of a single cell cannot unequivocally describe the stimulus since the response from a single cell to the same stimulus has a considerable variability for different presentations. Moreover, the timing sequence differs not only in the time events but also in the spike rates, producing uncertainty in the decoding process. Secondly, the same sequence of neuronal events in an aisle cell may be obtained by providing different stimuli, introducing ambiguity in the neuronal response.

New recording techniques arisen from emerging technologies, allow simultaneous recordings from large populations of retinal ganglion cells. At this time, recordings in the order of a hundred simultaneous spike trains may be obtained. New tools for analysing this huge volume of data must be used and turn out to be critical for proper conclusions. FitzHugh used a statistical analyser which, applied to neural data was able to estimate stimulus features. Different approaches have been proposed on the construction of such a functional population-oriented analizer, including information theory, linear filters, discriminant analysis and neural networks.

Analyzing the neural code, especially when this code is split by clustering algorithms in the search of certain levels of organization within it, implies to quantify the amount of

information each cell conveys. The goal of this study was to quantify the ganglion cells tendency to group themselves in sets of relatives according to their coding performance, using functional clustering (FC), information theory (IT) and artificial neural networks (ANN) as tools for providing an empirical value for the goodness of a coding capability. Therefore, a functional separation, or classification based on behaviour, was accomplished and the coding abilities of the subsets and the whole cluster of cells determined. Finally the strong relationship between stimulus reconstruction using artificial neural networks and mean cell information provided by information theory was proved.

In this chapter, we analyse the retinal population data looking at behaviour and exploring the contribution that single cells or population of cells make to the coding process. Two approaches have been used for this purpose: ANNs and IT. Each method required slightly different experimental paradigms that will be explained below.

Firstly, we have tested the ANN performances that small population of ganglion cells achieved at predicting stimuli of varying intensity and wavelength. We have compared at this point individual and population performances for each of the two experimental setups: intensity and wavelength variations. We have also looked at the ANN prediction performance of relevant parameters in the code such as firing rate, latency of first spike, latency of second spike and inter-spike interval. Two different network architectures were studied: Backpropagation and Kohonen Learning Vector Quantization (LVQ).

Secondly, entire populations of ganglion cells were reorganised in a varying number of subsets of cells (subpopulations). The method consisted of creating population subsets using the autocorrelograms of the cells and grouping them according to a minimal Euclidian distance. These subpopulations share functional properties (periodicity) and may be used for data reduction, extracting the relevant information from the code. Information theory and artificial neural networks have been used to quantify the coding goodness of every subpopulation, showing a strong correlation between both methods. All cells that belonged to a certain subpopulation showed very small variances in the information they conveyed while these values were significantly different across subpopulations, suggesting that the functional separation worked around the capacity of each cell to code different stimuli.

## 2. Methods

### 2.1 Experimental procedures

Extracellular recordings were obtained from ganglion cell populations in isolated superfused albino rabbit (Oryctolagus cuniculus) retina using a rectangular array of 100, 1.5 mm long electrodes, as reported previously (Fernandez et al., 2000; Normann et al., 2001a; Ortega et al., 2004; Bonomini et al., 2005). Briefly, after enucleation of the eye, the eyeball was hemisected with a razor blade, and the cornea and lens were separated from the posterior half. The retinas were then carefully removed from the remaining eyecup with the pigment epithelium, mounted on a glass slide ganglion cell side up and covered with a Milipore filter. This preparation was then mounted on a recording chamber and superfused with bicarbonate-buffered Ames medium at 35ºC.

For visual stimulation we used a 17" NEC high-resolution RGB monitor. Pictures were focused with the help of lens onto the photoreceptor layer. The retinas were flashed periodically with full field white light whereas the electrode array was lowered into the retina until a significant number of electrodes detected light evoked single and multiunit responses. This allowed us to record with 60-70 electrodes on average during each

experiment. The electrode array was connected to a 100 channel amplifier (low and high corner frequencies of 250 and 7500 Hz) and a digital signal processor based data acquisition system. Neural spike events were detected by comparing the instantaneous electrode signal to level thresholds set for each data channel using standard procedures described elsewhere (Fernandez et al., 2000; Normann et al., 2001a; Shoham et al., 2003). When a supra-threshold event occurs, the signal window surrounding the event is time-stamped and stored for later, offline analysis. All the selected channels of data as well as the state of the visual stimulus were digitized with a commercial multiplexed A/D board data acquisition system (Bionic Technologies, Inc) and stored digitally.

For spike sorting we used a free program, NEV2lkit, which has been recently developed by our group (Bongard et al., 2004) and runs under Windows, MacOSX and Linux (source code and documentation is freely available at: http://nev2lkit.sourceforge.net/). NEV2kit loads multielectrode data files in various formats (ASCII based formats, LabView formats, Neural Event Files, etc) and is able to sort extracted spikes from large sets of data. The sorting is done using principal component analysis (PCA) and can be performed simultaneously on many records from the same experiment.

### 2.2 Visual stimulation

Initially light stimulation was applied using a halogen light lamp, selecting the wavelength by means of narrow bandpass interference filters. Intensity was fixed by using neutral density filters and a shutter provided the the stimuli flashes to the preparation. In order to place the array in the optimum recording situation, the retina was stimulated with full field flashes of constant intensity while the array was lowered towards the preparation. The multiarray was then fixed at the place of maximum retinal response.

For the ANN experimental paradigm, stimulation consisted of seven consecutive flashes, with 250 msec. length. In this case, the wavelength and the intensity was varied separatedely. This is, a first run of flashes with changing intensity was presented and afterwards, a second protocol of varying wavelengths showed flashes to the retina. The fifteen most responsive units were selected for analysis.

For the IT experimental paradigm, retinas were randomly stimulated with full field flashes with 16 different light intensities within the grey scale. In order to ensure that both the number of trials for each intensity and the probabilities of appearance of each intensity was equal, a lookup table with 16 light intensities equally distributed, ranging from black (RGB values: 0, 0, 0) to white (RGB values: 255, 255, 255), was constructed. Afterwards, the

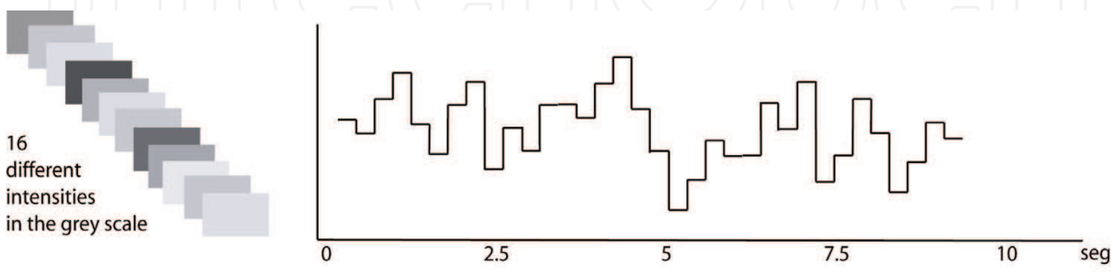


Fig. 1. Visual stimulation. Light intensity trace for 9 seconds of a sample trial containing 30 flashes, each lasting 0.3 ms. Ordinate axis represent the different intensity values (see methods).

elements of a list containing 20 repetitions for each of the intensities from the lookup table were relocated by changing their indexes according to a random entry chosen from a uniform distribution. The list was then loaded by a Python (http://www.python.org) script and embedded in VisionEgg (http://www.visionegg.org) for presentation of the flashes. Flashes were 300 ms long so that each trial lasted 96 seconds. Figure 1 shows one example of the light intensity trace.

### 2.3 Separation into subpopulations

In order to identify classes or groups of neurons that behave similarly we used DATAMEAns, a free open-source software for the classification and management of neural ensemble data (Bonomini et al., 2005) which is freely available from the following URL: http://cortivis.umh.es. We tested two spike train analysis methods, namely autocorrelations and post-stimulus time histograms (PSTHs). The outputs of this analysis fed then a non supervised clustering method, which used the nearest-neighbour or *k*-means approach for the creation of a varying number of autocorrelograms or PSTH groups. This is a simple clustering method that decomposes the data set into a set of disjoint clusters and then minimizes the dissimilarity in the samples within each cluster, while maximizes the dissimilarity of different clusters. As measure of dissimilarity we used the average squared distance of the data items from their nearest cluster centroids. This procedure defined a set of implicit decision boundaries for the separation of clusters or groups of units according to their periodicity. In this way, we ended up with several clusters or groups of ganglion cells that were a subset of the entire population.

In order to prove that functional clustering produced a reorganization of the cells around coding ability, two different control groups were defined as follows. The first control group was a set of subpopulations resulted from the clustering of the raw data (spike trains without any processing) instead of clustering the functional data (autocorrelograms or PSTHs). In the second control group, on the other hand, subpopulations were originated from a random arrangement. Each cell response was assigned a number and different subpopulations were constructed by picking up the spike train corresponding to a number originated from a random process, resembling a lottery process.

### 2.4 Neural Networks

For the analysis stage, 15 electrodes with highest activity (high level to noise ratio) were used, while the sixteenth channel was used for storing the original stimulus. For each electrode a 4-element vector was constructed using the number of spikes, the relative time of the first and second spike, and the interspike interval of these firings, building a 60-element vector with the concatenation of the 15 electrode 4-element vectors.

Two different neural networks were used. The first one was a three layer backpropagation, which receive the 60 elements or the four parameters of a single cell, with 20 nodes in the hidden layer, and the output layer consisting in the same number of neurons as the classes to be recognized. So each neuron just fires by applying a certain stimulus response, and the rest of the neurons of the output layer have no activation, acting as a winner-take-all network. The activation function used for all neurons, including the output layer was the hyperbolic tangent sigmoid transfer function given by:

$$f(x) = \frac{2}{1 + e^{-2x}} - 1 \tag{1}$$

using as initial momentum and adaptive learning rate the values established by default by Matlab Neural Network Toolbox, the initial weights randomly initialized and the network trained to minimize a sum square error goal of 1, to provide more generality in the recognition stage.

The other network used was the Kohonen Supervised Learning Vector Quantization (LVQ) with 16 neurons in the competitive map, and a learning rate of 0.05. This network is a competitive network, where the neurons with weights more similar to the input increase their strength, decreasing the rest of the nodes except a close neighborhood, establishing in this way topological relations in the map. The main advantage of using learning vector quantization is that it takes shorter to reach the convergence criteria.

Once the network has been trained, the recognition stage with extended data was accomplished, and the correlation coefficients between the stimulus and its estimation computed. It is important to mention that correlation gives a better estimation of the relation between the estimation and the known applied intensity or wavelength, than an absolute recognition rate, because the difference between two similar stimuli is very small, so the network can easily estimates any one of them. Other studies use their own concepts as mutual information in order to assess the overall quality of the reconstruction, but there no exist a common agreement about the measure that better estimate the goodness of the prediction.

### 2.5 Information theory

Information theory (Shannon, 1948) was used to assess the quality and reliability of the subpopulations obtained. This approach allows to answer questions about the relevant parameters that transmit information as well as addresses related issues such as the redundancy, the minimum number of neurons needed for coding certain group of stimuli, the efficiency of the code, the maximum information that a given code is able to transmit and the redundancy degree that exists in the population firing pattern (Borst and Theunissen, 1999; Amigo et al., 2003; Panzeri et al., 2003; Pola et al., 2003). We analysed the information about the stimulus that single cells conveyed, as well as the progression of the mutual information values after increasing the number of cells for each subpopulation. For it, the population responses of the retina under several repetitions of the stimuli were discretized into bins. Then, the firing rates from the cells of the population implemented a vector $n$ of spikes counts, with an observed probability $P(n)$. Since the probability of the occurrence of different stimuli had a known probability $P(s)$, the joint probability distribution can be defined as the probability of a global response $n$ and a stimulus $s$, $P(s,n)$. Thus, the information provided by the population of neurons about the stimulus is given by:

$$I(t) = \sum_{s \in S} \sum_{n} P(s,n) \log_2 \frac{P(s,n)}{P(s)P(n)} \tag{2}$$

From the above mentioned data, two informational indicators were constructed: the *mean cell information (MCI)*, calculated as the sum of the mutual information of each isolated cell divided by the total number of cells in a particular subpopulation, and the *subpopulation information (SI)*, defined as the overall mutual information for a given subpopulation (all the cells that belong to the subpopulation are taken into account). Note that these indicators are conceptually separated, since one points out to individual coding abilities (MCI) while the other refers to synergic coding abilities (SI).

## 3. Results

### 3.1 Population coding and ANNs

The fifteen electrodes with highest activities were selected for the analysis stage. Temporal coding or population coding are possible candidates for representing the stimuli. Another firing characteristic is that for a given cell, no unique response is obtained to the same stimulus. It can be observed that different presentations for the same stimuli evoke different responses, not only on the number of spikes but also on the relative timing of the firings, manifesting variability in their spiking behavior. This variability produces *uncertainty* for recognizing the right stimuli just using the spiking parameters, because there no exists an unequivocal function that associates the firing variables with the provided visual information in an aisle cell.

*Ambiguity* is another aspect noticed, a single cell can respond exactly the same to different stimuli, making more difficult, as for variability, their recognition. We point to a population coding as a candidate strategy for representing information in the visual system. The overall contribution of an aisle cell was compared with the recognition correlation scores for discriminating different intensities obtained using the fifteen cells. The firing parameters used were the number of spikes, the time of the first and the second spike during the ON stimulus, and the interspike interval. Figure 2 shows the correlation between the output of a trained backpropagation neural network and the correct stimuli, which consisted in 8 different intensities. The stimuli wavelength was fixed to 633, 546 and 450 nm. respectively in order to not influence the intensity transmitted. It can be seen that the scores show variability depending on the wavelength provided. The cells with higher recognition scores are cells 8, 10, 11 and 12 for all stimuli. While these cells had registered the maximum number of spikes, and there is a close relation between the number of spikes and the intensity, it seems reasonable that these cells obtain the higher scores. However using all cells the recognition index overpass 0.95 for all wavelengths.

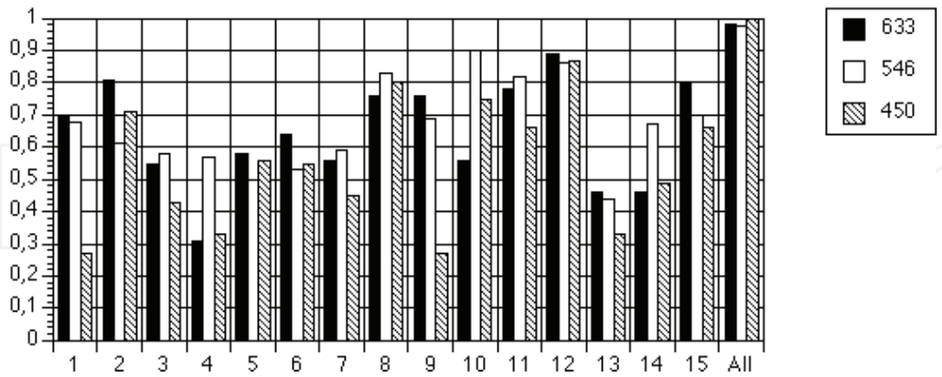


Fig. 2. Intensity recognition scores for aisle cells and the whole population using a BP network

Color recognition is more complex, and the recognition rates for aisle cell are much lower. Intensities were fixed to 1, 1.5 and 2 log units, and nine wavelengths had to be discriminated. Again the scores are variable according with the intensity. The population score, which lies in the range of 0.95, clearly surpass all the individual indexes for all kind of stimuli.

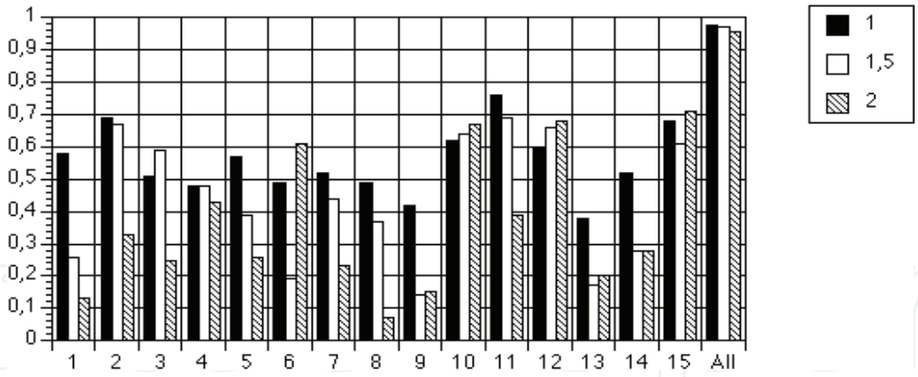


Fig. 3. Color recognition scores for aisle cells and the whole population using a BP network

For validating the prior results, the same data was presented to another kind of neural network, a supervised learning vector quantization (LVQ) with 20 nodes in the competitive layer. This network took lower time to converge than the prior one, and again, the correlation indexes between the correct stimulus and the estimation provided by the network were computed. The cells with higher recognition scores, cells 8, 10, 11 and 12, were the most successful in their estimations alone, and the population index was nearly the same that the one obtained using back-propagation networks for all kind of wavelength (633, 546 and 450 nm.), in the range of 0.95, confirming the recognizing capabilities of the population code.

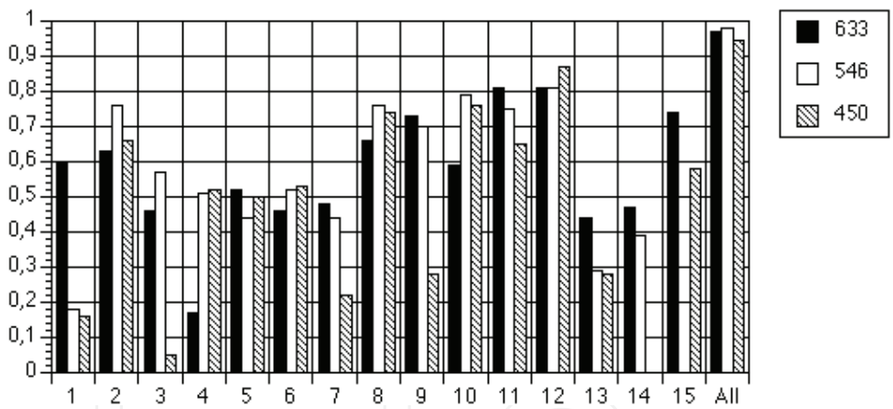


Fig. 4. Intensity recognition scores for aisle cells and the whole population using a LVQ network

The wavelength discrimination using competitive networks behaves similar to the prior feedfoward network. Lower recognition scores are obtained, even for the neural population, (this may be due to the network difficulty to fix a decision border which divides the different clusters) however this value is clearly higher that the correlation rates obtained by the cells alone. Using different neural networks does not affect to the obtained results, in respect to the most discriminating cells, and the higher scores obtained by the population parameters.

Once the population code has been noted as the most discriminant element in the neural firing, it still remain to define which are the parameters embedded in the neural signal that are used by cells for transmitting the data. A backpropagation network with 20 nodes in the hidden layer was used, and the input to this layer consists in the 15 population cells aisle parameters in contrast to the whole set of parameters. Figure 6 shows the correlation indexes between the correct stimuli and the network estimations. It can be seen that using

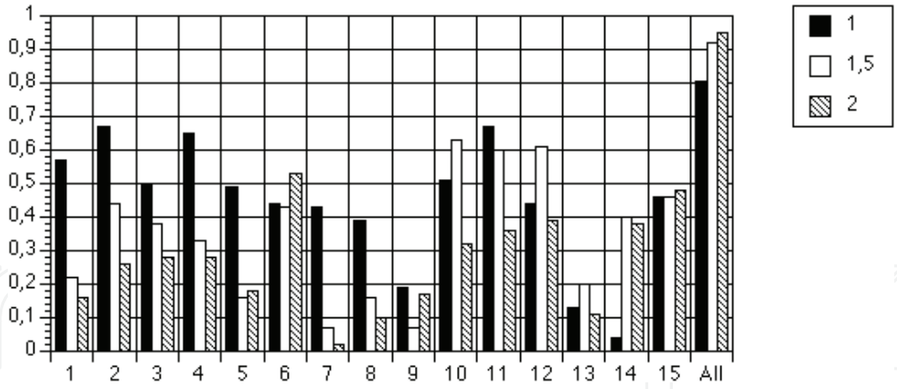


Fig. 5. Color recognition scores for aisle cells and the whole population using a LVQ network

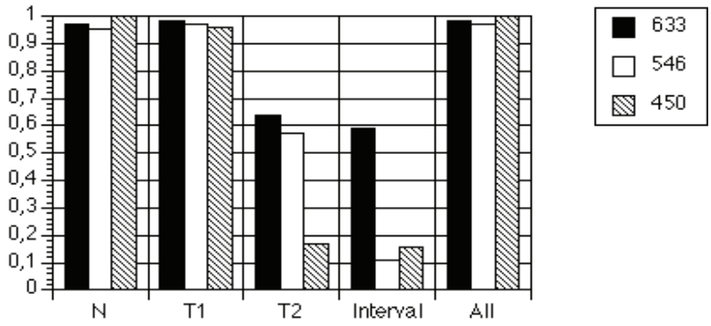


Fig. 6. Intensity recognition scores for the population using the parameters alone and the whole set in a BP network

only the number of spikes of the population is enough for recognizing successfully a given intensity (it has been described in literature the relation between the intensity level and the number of firing rate evoked), but also using only the exact timing of the first spike in all cells is enough for recognizing the stimuli for all wavelengths (lower intensities show longer delays). The second spike timing carries less information, and the interspike data is also a poor coding element.

The relative relevance of the aisle population parameters on recognizing colors was also computed. A backpropagation network was again used, showing similar results that the ones obtained for recognizing intensities. Just using the number of spikes of the whole population is enough for determining the provided color, and the time first spike occurs

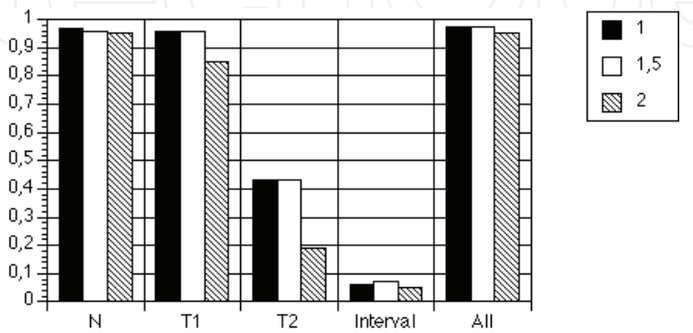


Fig. 7. Color recognition scores for the population using the parameters alone and the whole set in a BP network.

also discriminate between the different provided wavelengths for all kind of intensities used. The time of the second spike during the ON period or the interspike interval show lower recognizing scores than previous parameters.

### 3.2 Entire population and subpopulations obtained

The classification algorithm worked around the coding abilities of the cells. This is, the subsets emerged from the original population with very different MCI values. The clearest clustering strategy showed up when separating autocorrelograms. Although PSTHs performed well, the MCI separation across subpopulations suffered a little bit. Figure 8 illustrates this fact, and the fact that subpopulations originated randomly (first control group) did not evidence this feature. Neither did the second control group, the clustering of raw data, since no useful subpopulations were even generated. Notice that most of the points in the bottom-right panel are coloured green.

The generation of subpopulations using the autocorrelogram approach is illustrated in Figure 9 with an example where the maximum number of clusters was fixed to three. Top panel displays the raster plot of the whole population of ganglion cells while bottom panels show the raster plots of different subpopulations (named s1, s2 and s3) obtained by applying a bin size of 10 ms and a maximum shift of 900 lags. Subpopulations are reordered so that *s1* is the subpopulation with fewer cells and subsequent subpopulations (s2 and s3) contain an increasing number of cells. Clear differences among the different subpopulations can be perceived. These differences were related mainly to the firing patterns and to the number of cells in each subpopulation. For instance *s1*, contained very few cells that fired almost constantly during the presentation of the stimuli, *s2* contained a considerable number of cells with apparent temporal patterns and *s3* was integrated by a higher number of cells which showed a more randomised activity.

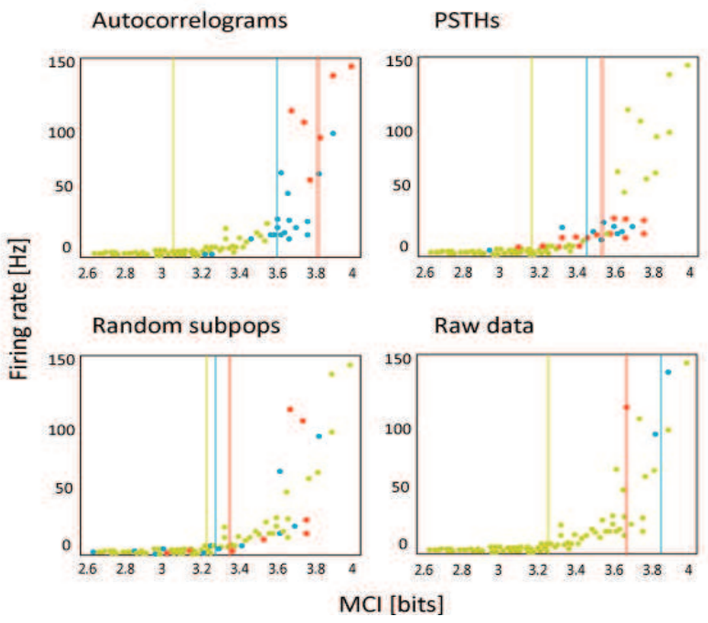


Fig. 8. Firing rate (Y axis) and MCI levels (X axis). Firing rates against MCI values for a collection of cells grouped into three subpopulations. Classes are indicated on different colours. Top left: autocorrelation approach. Top right: PSTH approach. Bottom left: random subpopulations. Bottom right: raw data.

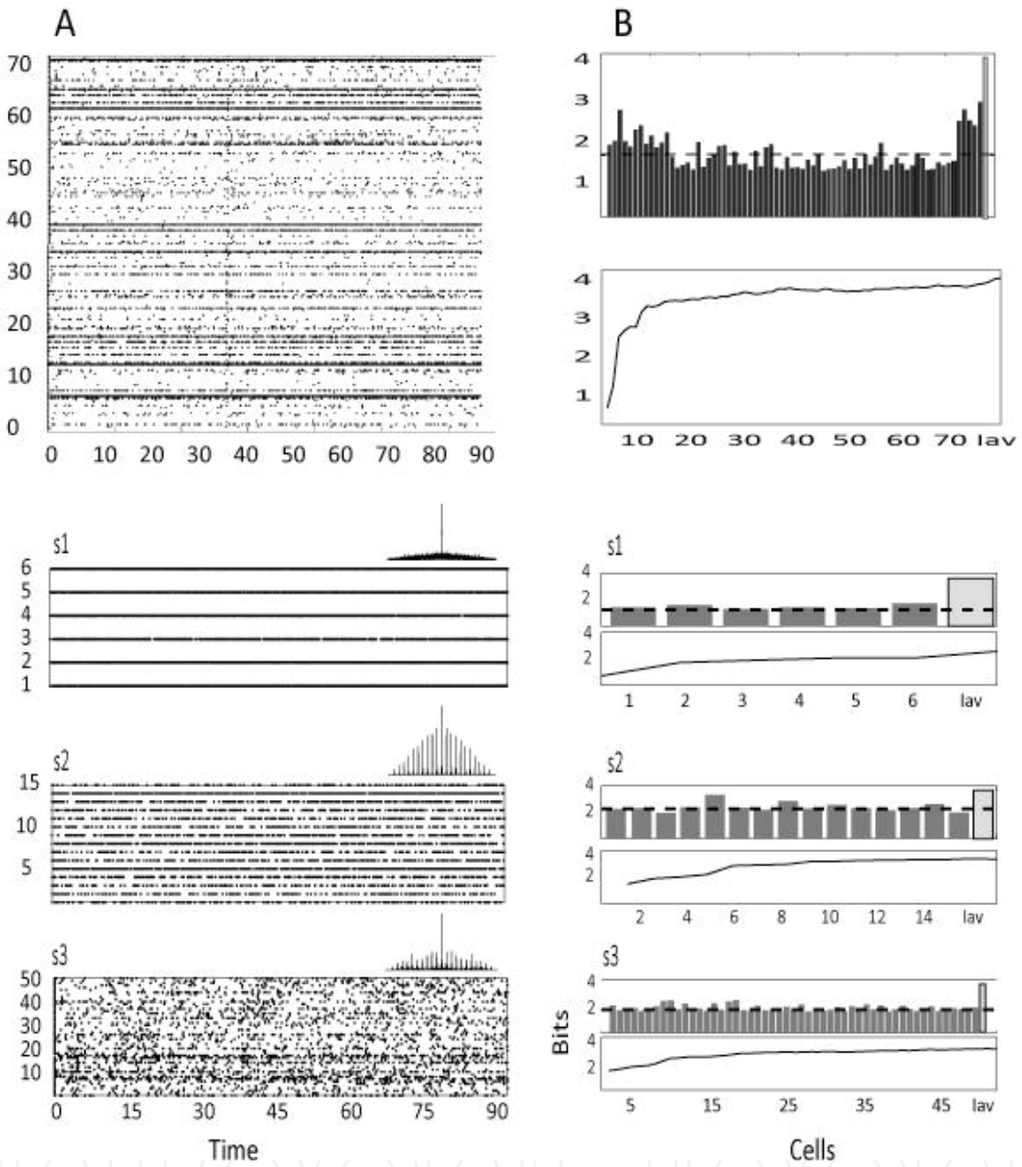


Fig. 9. *Top panel.* Example of simultaneously recorded extracellular responses from a population of rabbit ganglion cells to a trial of random full field flashes with 16 different intensities (see methods). (A) Original population raster plot. Each dot represents a single spike. (B) Mutual information values for each cell in the recording (bars) and for the whole population (last gray bar). The overall *mean cell information* is shown as a dashed line. (C) Accumulative mutual information for an increased number of cells. In this example the number of cluster was fixed to three. *Bottom panel, left.* Raster plots for each subpopulation (named s1, s2 and s3). *Bottom panel, right.* Information about the stimulus for the subpopulations. Mutual information values for each cell in the recording (bars) and for the whole subpopulation (last gray bar). The overall *mean cell information* in each case is shown as a dashed line. Bellow each bar graph it is displayed the accumulative mutual information for an increasing number of cells. Note the relationship between number of cells and *mean cell information*.

### 3.3 Quality of the subpopulations: information theory approach

Using the autocorrelogram approach the subpopulation information (SI), kept similar across classes (one-way ANOVA; p=0.82) while the informative value of the individual cells, summarised by the mean cell information (MCI) varied significantly (one-way ANOVA; p<0.0005). The PSTH approach was less effective at grouping subpopulations on an informational basis, even though the above trend was evident in the subpopulations separation.

Figure 9 (bottom panel, right) shows the information that each cell conveyed about the stimulus (black bars), their mean value (MCI, dashed line) and the SI value (grey bar) for different subpopulations arisen for k set to 3. Notice the difference in the *MCI* and *SI* values. As expected, s1, formed by the very few continuously firing cells gave the lowest *mean cell information* (1.48±0.10 bits; M±SE), clearly above the overall value of the whole population (2.42±0.08 bits; M±SE) whereas *s2*, kept the moderately informative cells (1.88±0.07 bits; M ±SE) and *s3* grouped the worst cells on a mean information basis (1.33±0.02 bits; M±SE). On top of each raster plot there is a pattern of the autocorrelogram representative of the subpopulation.

Taking apart the noisy cells, a particular relation between number of cells and MCI was found. Although the number of cells did not affect the *subpopulation information*, this measure was inversely correlated with the *mean cell information*. Therefore, the subpopulations with fewer cells tended to have higher *mean cell information* values. Figure 10 illustrates this fact. Here, MCI values obtained with *k* ranging from 2 to 5 are collected and plotted versus the number of cells, *n*. It can be observed that the *mean cell information* decreases as the number of cells in a certain subpopulation increases, fitting this relationship to a linear equation, with square r going from major to minor through autocorrelograms, PSTHs and control group (raw data), respectively. It is important to notice that the latter behaviour does not hold for the *subpopulation information*, which keeps invariant for any cell number. Note the strength of this observation for the autocorrelogram approach (upper panel), and how this behaviour suffers with the PSTH approach (middle panel) until is completely faded when raw data, where no temporal feature was taken into account before the clustering procedure.

We also found out that there is a natural number of subpopulations which optimise the clustering strategy. Such critical value for the number of groups (*k)* can be appreciated on Figure 11, where the clustering is shown on an informational basis. MCI and SI values for subpopulations obtained by processing ten original populations by means of the autocorrelogram approach are collected and displayed for an increasing number of classes (*k*). In this figure, subpopulations belonging to a certain class are represented with the same marker through different values of *k*. On the x-axis are displayed the *MCI* values and on the y-axis the *SI* values. Note that although for *k*=4 the two central clusters start to overlap, this is, subpopulations start to share MCI levels, the goodness in the group separation when taking the autocorrelogram approach is still evident. However, for five sets of relatives, the clustering behaviour becomes totally blurred and redundant subpopulations start to generate. Left panels contain data obtained with the autocorrelogram approach while right ones display data from the PSTH approach. Unlike the autocorrelograms, the PSTH approach fails to produce a robust separation according to information features for *k* greater than two. Thus, for 3 classes on, clusters start to spread and overlap. This could imply that PSTHs have a natural *k* much lower than autocorrelograms, since they could tell less (extract less information) about the experimental paradigm proposed here. The *k* value is the

maximum number of predefined classes, but the algorithm finds the optimal number, lower or equal than this predefined value.

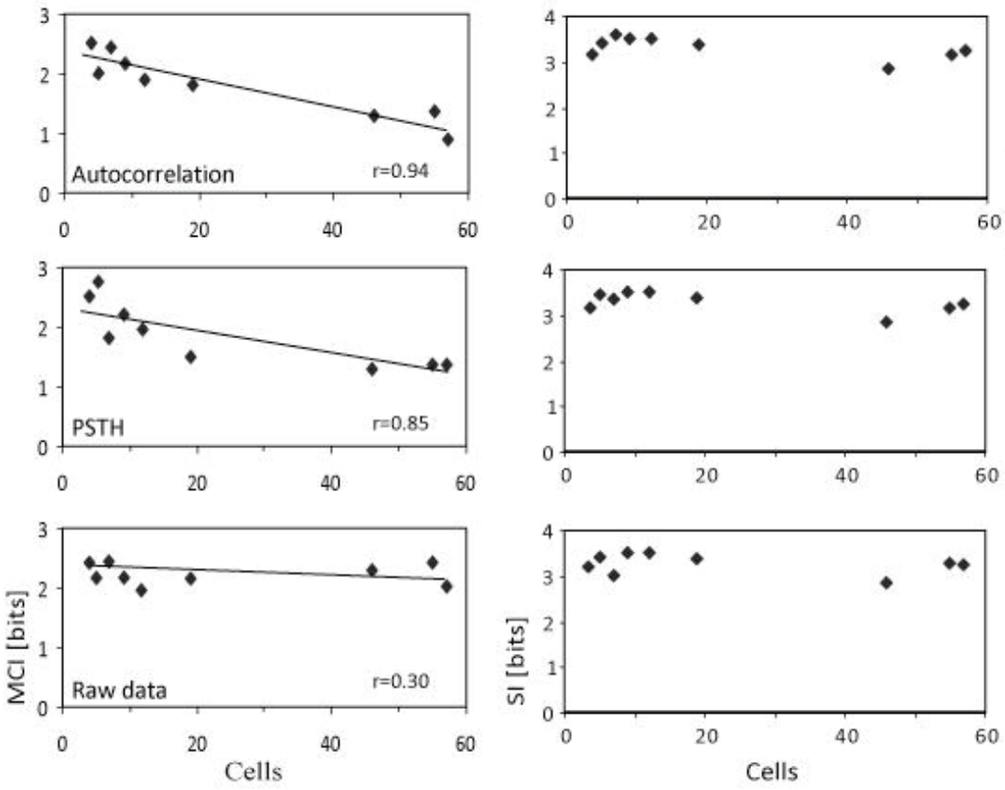


Fig. 10. Cell number versus coding quality. *Mean cell information (MCI)* against number of cells (*n*). Note that MCI decreases as the number of cells in a certain subpopulation increases. Upper panel: data obtained from the autocorrelogram approach. Middle panel: data obtained from the PSTH approach. Bottom panel: data obtained from raw data.

### 3.4 Correlations

We also looked for concerted activity within each subpopulation. In order to do so, a bin of 0.5 ms was used to be able to see peaks of concerted activity of 1 ms. Figure 12 describes how the method produces subpopulations with different levels of synchrony. Up to three main correlations widths were found: a narrow 5 ms peak, a 10 ms peak and a broad 30 ms peak. Subpopulations with highest MCI values showed either intermediate or broad correlation peaks and a smaller number of correlated cells. Continuously firing cells belonged to this latter group. Subpopulations containing the greatest number of correlated cells showed concerted activity around 5 ms but, surprisingly, the MCI values for these subpopulations were not the highest ones. This inverse relationship between synchronicity and individual informative value (MCI) is not surprising when looking at the overall information (SI), which kept constant across the different subpopulations, which in turn, presented SI values similar to the original population. This would suggest the coexistence of elements of both strategies, individual and population coding.

Raw data did not show any significant correlation. PSTH data, on the other hand, presented a weak separation of correlated cells with a narrow and a broad peak. Finally, autocorrelogram data, displayed a clear separation of the concerted activity giving place to a different peak for each subpopulation. Here, subpopulations were grouped according to their synchrony windows, from infinity (subpopulation with no correlation at all) to 30 ms.

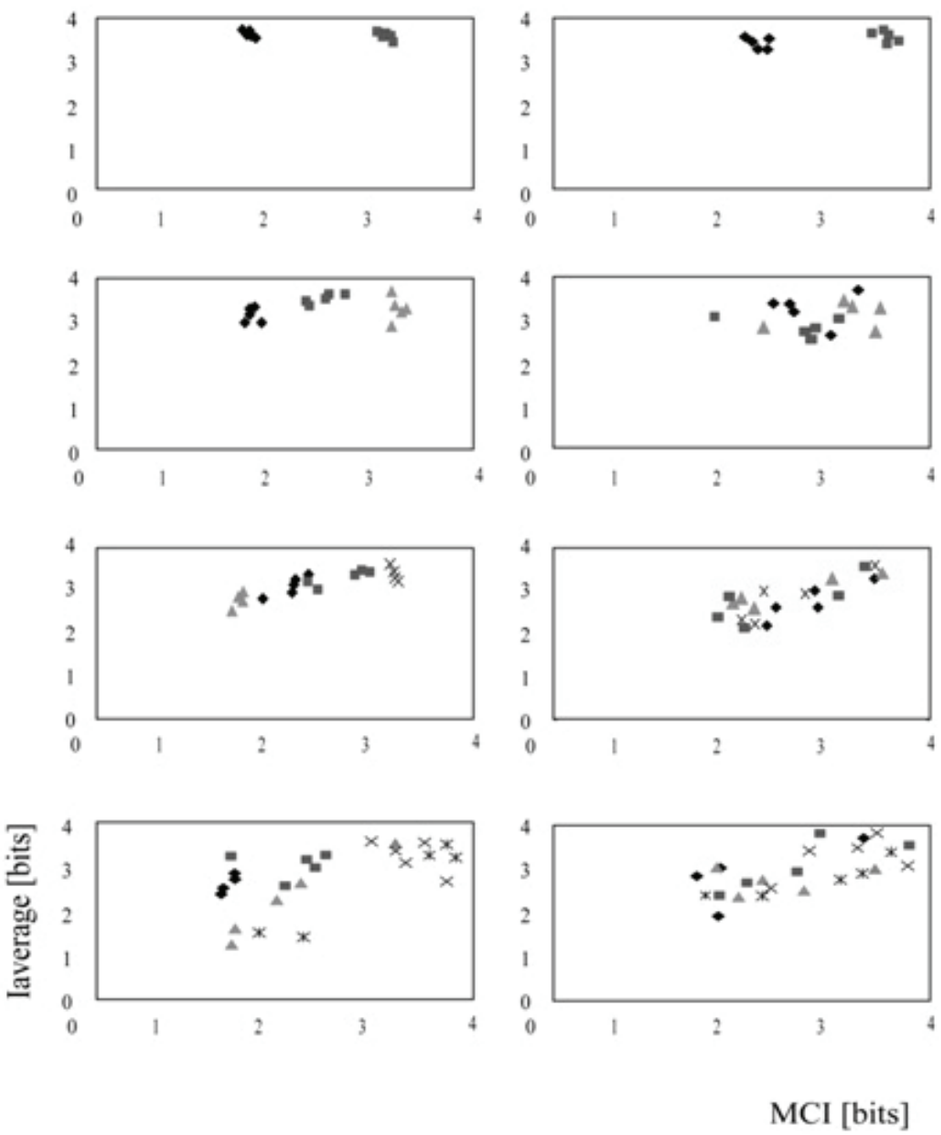


Fig. 11. Relationships between number of clusters and mean cell information values. Different trials are represented with different markers. Note that the individual components of each subpopulation have similar subpopulation information values and that there is a maximum number of clusters which optimise the classification strategy. Thus for $k$=4 although the two central clusters start to overlap, the group separation it is still apparent. For $k$=5, the clustering behaviour becomes totally blurred.

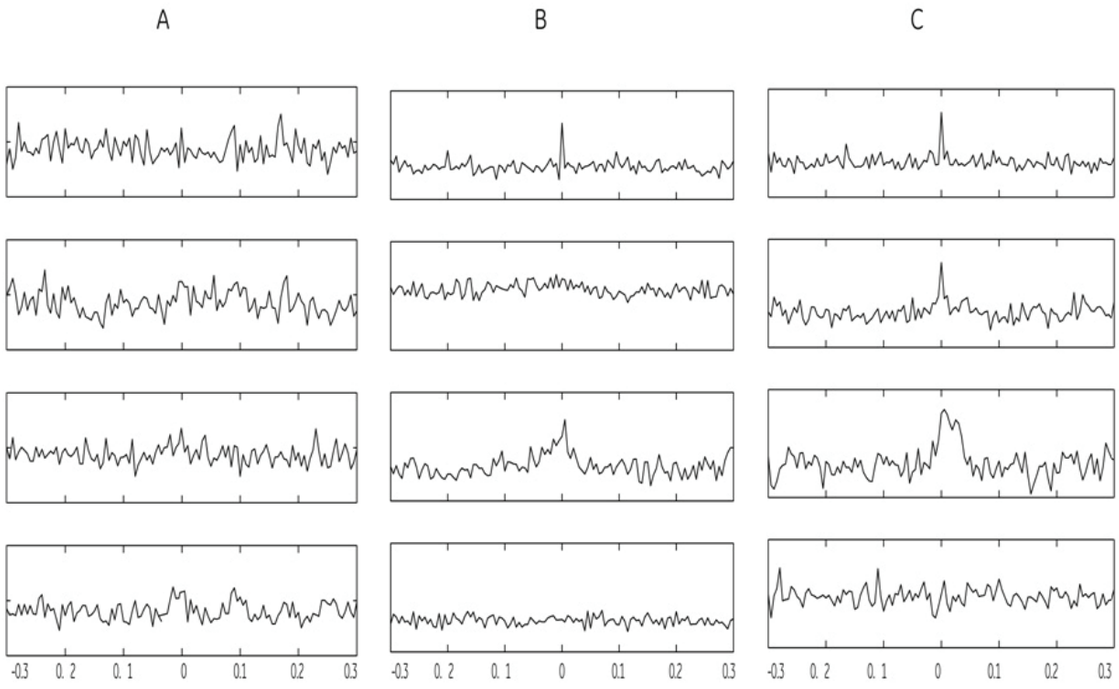


Fig. 12. Concerted activity of subpopulations. Each row represents the correlation signal of each subpopulation. Correlation were computed as the average of the correlation signals among all the cells belonging to that subpopulation in a pair wise process. Firing rate against MCI values. A), Data obtained from raw data. B), Data obtained from the PSTH approach. C), Data obtained from the autocorrelogram approach.

### 3.5 Artificial Neural Networks and information theory

In order to address quality differences across subpopulations, we used a feed-forward back-propagation neural network to study the contribution of the mean cell information indicator to group cells that are better encoders than others with respect to the stimulus applied. Interestingly, the neural network performance obtained with the different sets of cells within each subpopulation was found to be related to the mean cell information. With the aim of quantifying this relationship, ANN performance percentages were transformed to arcsin values and the mean cell information values underwent a logarithmic transformation in order to study the linearity of its relationship. Afterwards, correlation coefficient and regression analysis was applied to the data. Fixing $k$=5 (see methods), a highly significant positive correlation was found for s1 (r=0.9436, df=4), s2 (r=0.9785, df=4) and s3 (r=0.9261, df=4). Figure 13 shows the lines fitted by means of regression analysis on each of the subpopulations generated from the population shown on Figure 9. Dots represent the samples from which regression analysis was calculated. Equations for the respective line fittings and square r are included in the figures. Here, it is clearly shown the strong relationship between stimulus reconstruction and mean cell information.

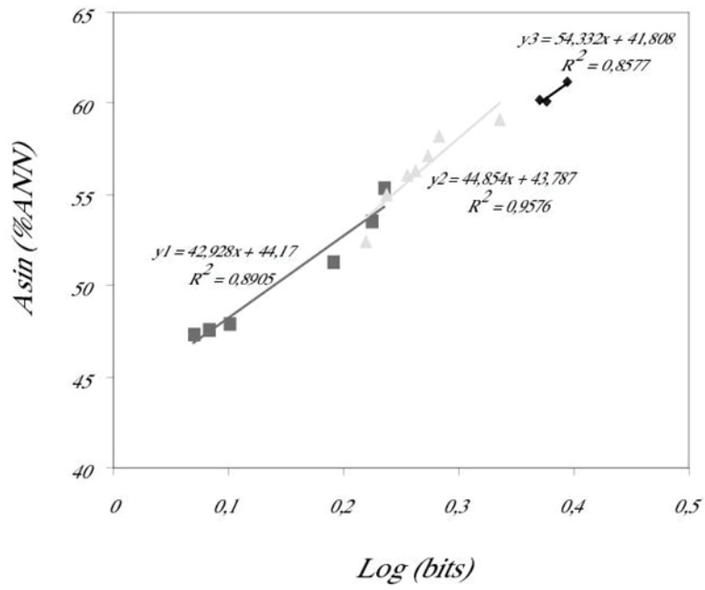


Fig. 13. ANN performance against mean cell information. Line fitting for s1 (squares), s2 (triangles) and s3 (rhombus). Notice that the best correlation coefficient belongs to the subpopulations with the best defined time patterns.

## 4. Discussion

The issue of classification has long been a central topic in the analysis of multielectrode data, either for spike sorting or for getting insight into interactions among ensembles of neurons (Fernandez et al., 2000; Nicolelis, 2003; Shoham et al., 2003; Carmena et al., 2005; Fernandez et al., 2005; Nicolelis, 2005; Suner et al., 2005; Hochberg et al., 2006).

A major challenge in this context is to acquire meaningful data from different functional types of neurons, but there is not a standard way for addressing how many neuronal types are in a given multielectrode recording. In this work we have introduced a new approach to facilitate this task which is easy to implement and has proved to be useful for defining subsets of retinal ganglion cells which share similar temporal responses and coding capabilities.

The fact that reliable separation of clusters was achieved does not mean that finer separation utilizing additional variables is not possible, but a clear trend in the clustering strategy was present for all the generated subpopulations. This might be explained from a functional point of view. Thus, we speculate with a natural number of retinal ganglion cell classes, where every class contributes to coding different elements of the visual scenario such as intensity, colour, texture, orientation, shape, etc (Kang et al., 2004). If the number of classes is increased the coding process could lose effectiveness, starting to turn up redundant classes or subpopulations. In other words, the classes would enclose different kind of cells with similar coding behaviour, like the intensity coders, colour coders and so on. Taking into account that the stimulus applied was intensity variation of full field flashes, the best coder subsets would effectively code intensity in these particular cases. However, this should be addressed in future works by repeating the visual stimuli with other varying parameters, for instance using different colours, moving bars, and even natural scenes to confirm such a functional separation. Additionally more sophisticated unsupervised clustering algorithms, particularly on the crucial issue of assessing the proper number of

clusters, are required and should be developed. Finally, some degree of controversy can accompany any classification scheme but we should take into account that the controversy is not concerned with whether the groups exist, or whether they are important; rather it is related to the number of groups to be present and the functional semantics attributed to them.

## 5. Acknowledgements

This research has been supported in part by grants Fundación Séneca 05732/PI/07, NAN2004-09306, SAF2005-08370-C02-01 and CIBER-BBN from the Spanish Government and by the European Commission through the project "NEUROPROBES IST-027017".

## 6. References

Amigo JM, Szczepanski J, Wajnryb E, Sanchez-Vives MV. On the number of states of the neuronal sources. Biosystems 2003; 68:57-66.

Bongard M, Micol D, Fernandez E (2004) Nev2lkit: a tool for handling neuronal event files. In: (http://nev2lkit.sourceforge.net/).

Bonomini MP, Ferrandez JM, Bolea JA, Fernandez E. DATA-MEAns: an open source tool for the classification and management of neural ensemble recordings. J Neurosci Methods 2005; 148:137-46.

Borst A, Theunissen FE. Information theory and neural coding. Nat Neurosci 1999; 2:947-57.

Cajal SR (1904) Textura del sistema nervioso del hombre y de los vertebrados. Madrid: Imprenta y librería de Nicolás Moya.

Carmena JM, Lebedev MA, Henriquez CS, Nicolelis MA. Stable ensemble performance with single-neuron variability during reaching movements in primates. J Neurosci 2005; 25:10712-6.

Costa L, Velte T. Automatic characterization and classification of ganglion cells from the salamander retina. J Comp Neurol 1999; 404:33-51.

Diaz E. A functional genomics guide to the galaxy of neuronal cell types. Nat Neurosci 2006; 9:99-107.

Egert U, Knott T, Schwarz C, Nawrot M, Brandt A, Rotter S, Diesmann M. MEATools: an open source toolbox for the analysis of multi-electrode data with MATLAB. J Neurosci Methods 2002; 117:33-42.

Fernandez E, Ferrandez J, Ammermuller J, Normann RA. Population coding in spike trains of simultaneously recorded retinal ganglion cells. Brain Res 2000; 887:222-9.

Fernandez E, Pelayo F, Romero S, Bongard M, Marin C, Alfaro A, Merabet L. Development of a cortical visual neuroprosthesis for the blind: the relevance of neuroplasticity. J Neural Eng 2005; 2:R1-R12.

Ferrández J, Bolea J, Ammermüller J, Normann R, Fernández E (1999) A Neural Network Approach for the Analysis of Multineural Recordings in Retinal Ganglion Cells: Towards Population Encoding. In: Lecture Notes on Computer Sciences (Verlag S, ed), pp 289-98.

Golledge HD, Panzeri S, Zheng F, Pola G, Scannell JW, Giannikopoulos DV, Mason RJ, Tovee MJ, Young MP. Correlations, feature-binding and population coding in primary visual cortex. Neuroreport 2003; 14:1045-50.

Hochberg LR, Serruya MD, Friehs GM, Mukand JA, Saleh M, Caplan AH, Branner A, Chen D, Penn RD, Donoghue JP. Neuronal ensemble control of prosthetic devices by a human with tetraplegia. Nature 2006; 442:164-71.

Kang K, Shapley RM, Sompolinsky H. Information tuning of populations of neurons in primary visual cortex. J Neurosci 2004; 24:3726-35.

Keat J, Reinagel P, Reid RC, Meister M. Predicting every spike: a model for the responses of visual neurons. Neuron 2001; 30:803-17.

Kim SJ, Manyam SC, Warren DJ, Normann RA. Electrophysiological Mapping of Cat Primary Auditory Cortex with Multielectrode Arrays. Ann Biomed Eng 2006.

Lehmkuhle MJ, Normann RA, Maynard EM. Trial-by-trial discrimination of three enantiomer pairs by neural ensembles in mammalian olfactory bulb. J Neurophysiol 2006; 95:1369-79.

McClelland J, Rumelhart D (1986) Explorations in Parallel Distributed Processing. Cambridge.

Meister M. Multineuronal codes in retinal signaling. Proc Natl Acad Sci U S A 1996; 93:609-14.

Meister M, Pine J, Baylor DA. Multi-neuronal signals from the retina: acquisition and analysis. J Neurosci Methods 1994; 51:95-106.

Migliore M, Shepherd G. Opinion: An integrated approach to classifying neuronal phenotypes. Nat Rev Neurosci 2005; 6:810-8.

Nicolelis MA. Brain-machine interfaces to restore motor function and probe neural circuits. Nat Rev Neurosci 2003; 4:417-22.

Nicolelis MA. Computing with thalamocortical ensembles during different behavioural states. J Physiol 2005; 566:37-47.

Normann R, Warren D, Ammermuller J, Fernandez E, Guillory S. High-resolution spatio-temporal mapping of visual pathways using multi-electrode arrays. Vision Res 2001a; 41:1261-75.

Normann RA, Warren DJ, Ammermuller J, Fernandez E, Guillory S. High-resolution spatio-temporal mapping of visual pathways using multi-electrode arrays. Vision Res 2001b; 41:1261-75.

Ortega G, Bongard M, Louis E, Fernandez E. Conditioned spikes: a simple and fast method to represent rates and temporal patterns in multielectrode recordings. J Neurosci Meth 2004; 133:135-41.

Panzeri S, Pola G, Petersen RS. Coding of sensory signals by neuronal populations: the role of correlated activity. Neuroscientist 2003; 9:175-80.

Pola G, Thiele A, Hoffmann KP, Panzeri S. An exact method to quantify the information transmitted by different mechanisms of correlational coding. Network 2003; 14:35-60.

Rieke F, Warland D, Van Steveninck R, Bialek W (1997) Spikes: Exploring the Neural Code. Cambridge.

Shannon C. A Mathematical Theory of Communication. Bell sys Tech 1948; 27:379- 423.

Shoham S, Fellows M, Normann R. Robust, automatic spike sorting using mixtures of multivariate t-distributions. J Neurosci Meth 2003; 127:111-22.

Shoham S, Paninski LM, Fellows MR, Hatsopoulos NG, Donoghue JP, Normann RA. Statistical encoding model for a primary motor cortical brain-machine interface. IEEE Trans Biomed Eng 2005; 52:1312-22.

Suner S, Fellows MR, Vargas-Irwin C, Nakata GK, Donoghue JP. Reliability of signals from a chronically implanted, silicon-based electrode array in non-human primate primary motor cortex. IEEE Trans Neural Syst Rehabil Eng 2005; 13:524-41.

Warland D, Reinagel P, Meister M. Decoding Visual Information from a Population of Retinal Ganglion Cells. J Neurophysiol 1997a; 78:2336-50.

Warland DK, Reinagel P, Meister M. Decoding visual information from a population of retinal ganglion cells. J Neurophysiol 1997b; 78:2336-50.

Warren DJ, Fernandez E, Normann RA. High-resolution two-dimensional spatial mapping of cat striate cortex using a 100-microelectrode array. Neuroscience 2001; 105:19-31.

Xia Y, Turken U, Whitfield-Gabrieli S, Gabrieli J (2005) Knowledge-based classification of neuronal fibers in entire brain. In: Med Image Comput Assist Interv Int Conf Med Image Comput Comput Assist Interv, pp 205-12.

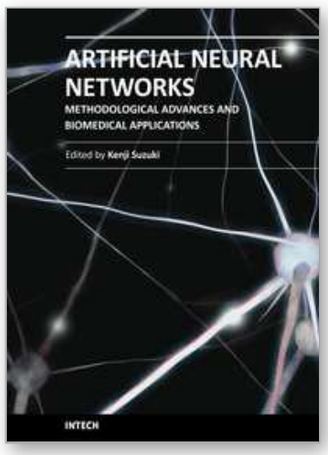


**Artificial Neural Networks - Methodological Advances and Biomedical Applications**

Edited by Prof. Kenji Suzuki

ISBN 978-953-307-243-2
Hard cover, 362 pages
**Publisher** InTech
**Published online** 11, April, 2011
**Published in print edition** April, 2011

Artificial neural networks may probably be the single most successful technology in the last two decades which has been widely used in a large variety of applications in various areas. The purpose of this book is to provide recent advances of artificial neural networks in biomedical applications. The book begins with fundamentals of artificial neural networks, which cover an introduction, design, and optimization. Advanced architectures for biomedical applications, which offer improved performance and desirable properties, follow. Parts continue with biological applications such as gene, plant biology, and stem cell, medical applications such as skin diseases, sclerosis, anesthesia, and physiotherapy, and clinical and other applications such as clinical outcome, telecare, and pre-med student failure prediction. Thus, this book will be a fundamental source of recent advances and applications of artificial neural networks in biomedical areas. The target audience includes professors and students in engineering and medical schools, researchers and engineers in biomedical industries, medical doctors, and healthcare professionals.

**How to reference**

In order to correctly reference this scholarly work, feel free to copy and paste the following:

María P. Bonomini, José M. Ferrández and Eduardo Fernández (2011). Artificial Neural Networks and Retinal Ganglion Cell Responses, Artificial Neural Networks - Methodological Advances and Biomedical Applications, Prof. Kenji Suzuki (Ed.), ISBN: 978-953-307-243-2, InTech, Available from: http://www.intechopen.com/books/artificial-neural-networks-methodological-advances-and-biomedical-applications/artificial-neural-networks-and-retinal-ganglion-cell-responses

INTECH
open science | open minds

**InTech Europe**
University Campus STeP Ri
Slavka Krautzeka 83/A
51000 Rijeka, Croatia
Phone: +385 (51) 770 447
Fax: +385 (51) 686 166
www.intechopen.com

**InTech China**
Unit 405, Office Block, Hotel Equatorial Shanghai
No.65, Yan An Road (West), Shanghai, 200040, China
中国上海市延安西路65号上海国际贵都大饭店办公楼405单元
Phone: +86-21-62489820
Fax: +86-21-62489821

IntechOpen